A Portable Nitrogen Dioxide Instrument Using Cavity-Enhanced Absorption Spectroscopy

Steven A. Bailey[1] , Reem A. Hannun[2], Andrew K. Swanson[1,3], Thomas F. Hanisco[1]

1. Atmospheric Chemistry and Dynamics Lab, NASA Goddard Spaceflight Center, Greenbelt, MD, USA
2. Atmospheric Science Branch, NASA Ames Research Center, Moffett Field, CA
3. SciGlob Instruments and Services, LLC, Columbia, MD, USA

Correspondence: Steven A. Bailey (steven.a.bailey@nasa.gov)

Abstract

The Portable (2.7 kg) Cavity-enhanced Absorption of Nitrogen Dioxide (PCAND) instrument for measuring *in situ* nitrogen dioxide (NO_2) was developed using incoherent, broadband cavity-enhanced absorption spectroscopy (IBBCEAS). An LED light source centered at 408 nm was coupled to a cavity 15 cm in length, achieving an effective optical pathlength of ~520 m. Precision was measured as 94 pptv (1 s). To date, we have flown this instrument on 3 balloon test flights. This instrument records data to an SD card and outputs data (via an RS232 port) to external devices including a commercial radiosonde (iMet) for real-time data downlink.

1 Introduction

Nitrogen dioxide (NO_2) is a major contributor to air pollution in the Earth's troposphere. Its main source is a byproduct of combustion from the burning of fossil fuels (Spinei, E. *et al.* 2014). NO_2 has been monitored from satellite instruments (like OMI, TROPOMI, and GEMS) for a decade (Miyazaki, K. *et al.* 2017, Duncan, B. *et al.* 2015, Martin, R.V. *et al*. 2003, Cooper, M.J. *et al.* 2020), providing a global understanding of emissions and air quality. However, satellite retrievals of the total column NO_2 rely on estimates of the vertical distribution of NO_2 based on models or climatology (Cersosimo, A. *et al*, 2020). These *a priori* estimates are a major source of uncertainty

in making retrievals of NO_2 columns from satellite measurements (Cooper, M.J. *et al*. 2020, Dang, R. *et al*. 2023).

Direct measurement of the vertical profile can verify and improve these *a priori* estimates. Aircraft instruments cannot typically make a continuous vertical profile of the atmospheric column. Therefore, an instrument with adequate precision that is small enough to fly on a balloon is needed. Typical concentrations of NO_2 range from a part per billion by volume (ppbv) in clean environments to several 10's of ppbv in polluted environments. A typical balloon ascent rate is 5 m/s, so a time response on the order of 10 s would give a 50 m resolution. An instrument sensitivity of less than a ppbv in 1 s integration is adequate to resolve the vertical distribution of NO_2 in a clean environment.

Existing compact sensors do not meet our requirements. Electrochemical sensors are widely used in low-cost sensor networks. These sensors meet the size and weight requirements to fly on a balloon, but they do not have the precision and accuracy needed for determining the vertical profile of NO_2. In addition, these electrochemical sensors do not have fast time response and not well-suited to changing environments. Kim, H., Müller, M., Henne, S., and Hüglin, C.: Long-term behavior and stability of calibration models for NO and NO_2low-cost sensors, Atmos. Meas. Tech., 15, 2979–2992, https://doi.org/10.5194/amt-15-2979-2022, 2022. Previously, a small NO_2 instrument was developed by the Royal Netherlands Meteorological Institute (Dutch: Koninklijk Nederlands Meteorologisch Instituut, KNMI) (Sluis, et al., 2010). That instrument uses chemiluminescence in a liquid solution to measure NO_2, with a reported precision of 7.7 ppbv/sec. Although this chemiluminescence instrument fits our size and weight criteria, it requires a lengthy calibration procedure before every flight and it does not have adequate sensitivity for our purposes.

Techniques for measuring in situ NO_2 with high precision in the atmosphere include Laser Induced Fluorescence (LIF) (Thornton, J.A. *et al.* 2000, optical absorption methods, like IBBCEAS (Womack, C.C. *et al.* 2022, Min K.E. *et al*. 2016), and chemical techniques, like chemiluminescence (Ryerson, T.B. *et al*. 2000). Although all these techniques have their pros and cons for use, we chose to focus on optical, absorption methods for several reasons. First, we have successful experience

using IBBCEAS in a previous ozone (O_3) based instrument (Hannun, *et al.*, 2020). Second, stability and ease of calibration are desirable, which we found to be the case with the O_3 instrument. Third, the technique can be scaled to a small enough size and weight to fly (via balloon) into the free troposphere. An instrument using LIF to measure NO_2 would (in our experience) not be suitable for our purposes. Its size and weight would be too great to work with a small weather balloon, despite LIF having greater sensitivity than IBBCEAS.

A description of PCAND follows. Performance metrics will show PCAND meets the Federal Aviation Administrations (FAA) uncontrolled, maximum allowable weight (~2.7 kg) for a balloon payload. In addition, PCAND sensitivity to NO_2 exceeds that from the KNMI sonde by more than an order of magnitude. A description of the PCAND calibration procedure is detailed showing its simplicity. An atmospheric vertical profile measurement from one of our balloon flights is shown. Finally, a ground-based validation of PCAND with another established NO_2 instrument is made.

2 Principle of operation

IBBCEAS is an established technique for the detection of trace gases (Fiedler *et al.*, 2003; Ball *et al.*, 2004; Washenfelder *et al.*, 2008) including NO_2 (Min *et al.*, 2016). PCAND uses an LED as the incoherent, broadband light source centered at 408 nm. This is coupled to an optical cavity with highly reflective mirrors on either end. IBBCEAS leverages the mirror reflectivity to turn a physically short path length (15 cm) of the cavity into an effective optical pathlength of ~520 m. This effective pathlength increases the probability of NO_2 absorption in the cavity, thereby increasing the sensitivity (94 pptv @ 1 s) of the instrument.

Shown in Fig. 1, output from an LED is collimated into the gas sample cell (cavity) where it first passes through the leftmost mirror. Both mirrors have highly reflective coatings (99.97%) on curved surfaces (r=250 mm) facing towards each other. Only a small fraction of light enters the cell, but the light (photons) bounces back and forth between both mirrors thousands of times on average before exiting the rightmost mirror. Photons that exit are then detected by a silicon

photomultiplier (SiPM). A transconductance amplifier is then used to convert small amounts of current from the SiPM into measurable voltage levels. A micro controller with a 12-bit analog to digital convertor digitizes this voltage. The micro controller is both a data acquisition system and a controller of the LED and 3-way valve. A digital lock-in scheme is used to remove background light by modulating the LED at 100 Hz with a large duty cycle (70%).

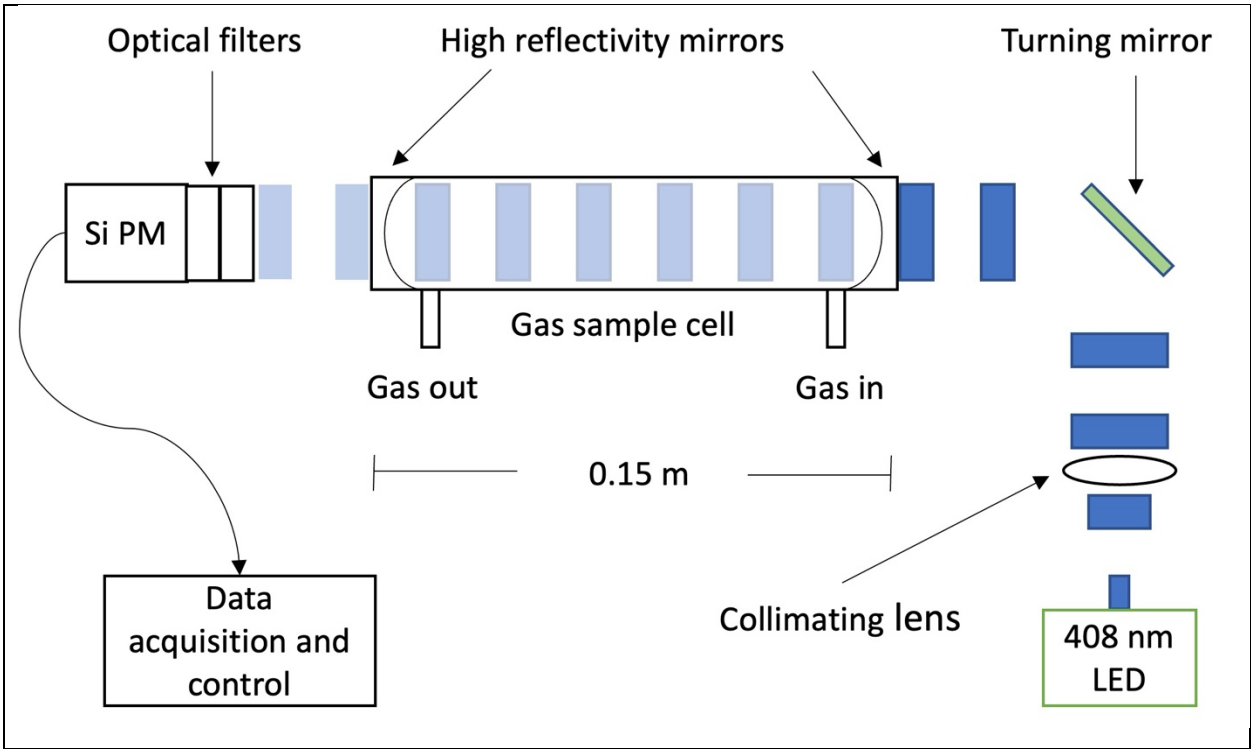

Figure 1. Incoherent broadband cavity enhanced detection technique for NO_2. An LED at 408 nm is collimated and coupled into the detection cell via high reflectivity mirrors (R = 99.97%), creating a long optical pathlength. The light attenuated by the sample is then detected using a silicon photomultiplier (SiPM).

Trace gas absorption (using IBBCEAS) is a measurement of light attenuation. As light is absorbed and scattered (via Rayleigh), an attenuation of light is seen at the SiPM. The Beer-Lambert absorption coefficient, α_{abs}, is directly related to the light intensity exiting the cavity (Washenfelder *et al.*, 2008; Hannun *et al.*, 2020) through the equations:

$$\alpha_{abs} = \left(\frac{I_0 - I}{I}\right)\left(\frac{1-R}{d} + \alpha_{Ray}\right) \quad (1)$$

$$\alpha_{cav} = \left(\frac{1-R}{d}\right) \quad (2)$$

$$L_{\text{eff}} = \left(\frac{1}{\alpha_{cav}}\right) \quad (3)$$

Here I_0 is the intensity of light in the absence of any absorbing molecules, I is the intensity of light including absorbing molecules, R is the mirror reflectivity, d is the physical distance between cavity mirrors, and α_{Ray} is the extinction due to Rayleigh scatter. The term $(1 - R)/d$ is the theoretical cavity loss, α_{cav}. L_{eff} represents the maximum effective pathlength. In the case of mirrors with R = 99.97%, the maximum theoretical L_{eff} for our 15 cm cell would be 450 m.

3 Instrument description

PCAND is housed in a small aluminum box measuring 38 cm length x 22 cm width x 7 cm height with a total weight of 2.7 kg. Inside the box (Fig. 2) is an optical plate where all the instrument components are mounted. Power comes from an 11.1 volt Lithium Ion rechargeable battery with 2200 mAh (24 Wh) of storage. Table 1 summarizes the PCAND design and performance characteristics.

Table 1. Summary of PCAND performance capabilities

Specification	Value
Size	38 x 22 x 7 cm
Weight	2.7 kg
Power	< 6 W
Data rate	1 Hz
Precision (1σ, 1Hz)	2.3 x 10^9 molec. cm^{-3}
Accuracy	6.0%
Time response	3 s

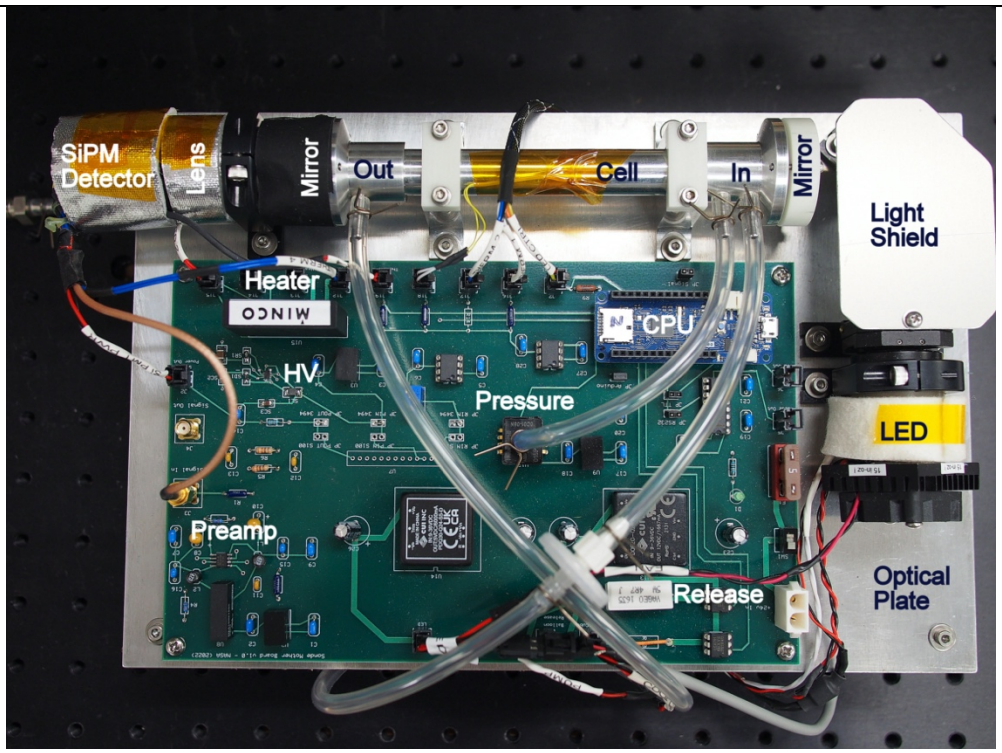

Figure 2. A top view of the NO_2 instrument. Major components include A) the optical plate, which consists of the LED assembly, light shield, turning mirror (under light shield), the optical cell, end mirrors, collimating lens, and SiPM detector; B) The electronics motherboard with detector preamp, heater controller, pressure sensor, balloon release circuit, and the data acquisition system (CPU). Not shown is the nafion tubing used to dry the air before entering the instrument.

3.1 Optical components

3.1.1 LED assembly

A UV LED (λ_{max} = 408 nm, FWHM = 30 nm) (Thorlabs M310D1) is mounted to a custom heat sink and temperature controlled to 25 °C with a thermo-electric cooler controller (Thorlabs MTD415T). Constant current to the LED is supplied by a low noise controller (Thorlabs MLD203CLN). The LED assembly includes a 15 mm focal length collimating lens (Thorlabs LA1074-A) followed by a turning mirror (Thorlabs PF10-03-F01) to direct light into the sample cell.

3.1.2 Sample cell

The sample cell is manufactured from an aluminum alloy tube measuring 15 cm in length with a 1.4 cm inner diameter. The cell mirrors (Layertec 103654) have a reflectivity of R = 99.97% over the detected spectral range (Fig. 3) and a 250 mm radius of curvature. Mirrors are held to the cell ends with bezel mounts on flanges with face seal o-ring glands. Although the mounts themselves are non-adjustable, they are fabricated to hold the mirrors in a way that maximizes their centricity to the cell ends. Furthermore, the incoherent light source negates the need for rigid mirror alignment. A pressure transducer (Honeywell ASDXACX015PAAA5) measures the cell pressure from a port near the cell inlet.

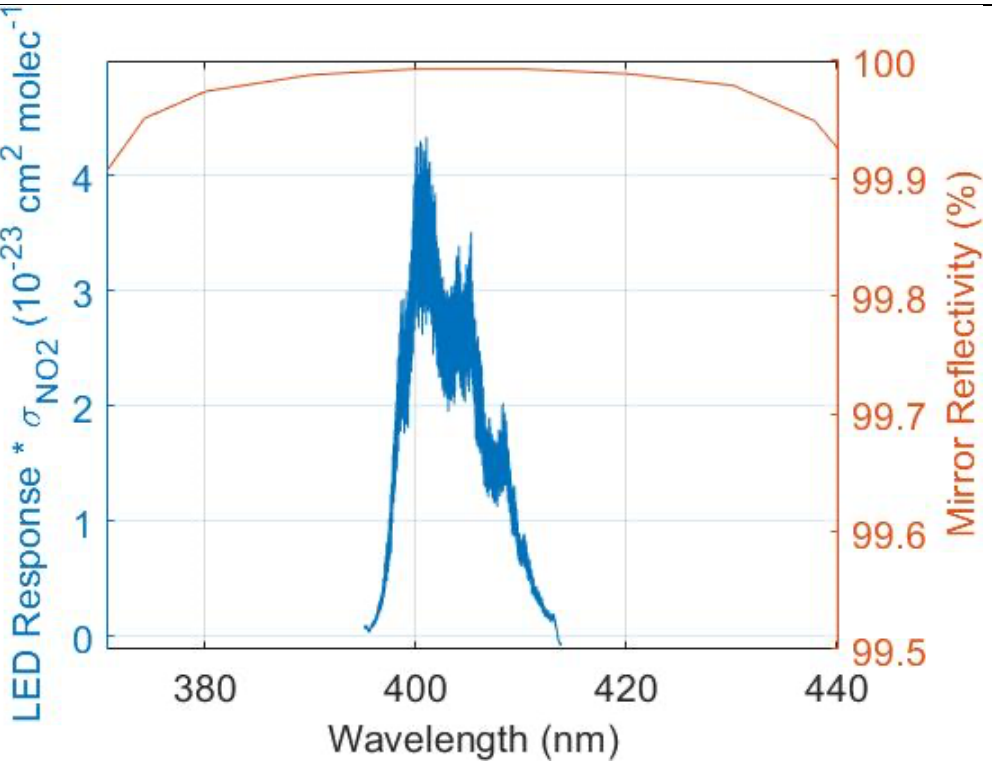

Figure 3. Normalized LED spectral response x NO_2 cross-section vs mirror reflectivity (99.97% @ 408 nm). The LED (λ_{max} = 408 nm, FWHM = 30 nm) response was measured using a grating spectrometer with the instrument SiPM and associated detector optics. The absorption cross-section of NO_2 (for this instrument) is the integration of the above product (with a resolution of 0.0005 nm) which yields 6.0419 x 10^{-19} cm^2 /molecule.

3.1.3 SiPM assembly

Following exit from the sample cell, light enters an optical bandpass filter (Semrock FF01-405/10-25), then a lens (Thorlabs LA1252-A) focuses the beam onto a Silicon Photo Multiplier (SiPM - Onsemi 30035) detector. The detector is biased by ~29 volts DC via a LT3494A boost converter. This voltage sets the gain of this device. Signal from the SiPM is amplified through a transimpedance amplifier based on a low noise, ADA4625-2 op-amp. The SiPM assembly is thermally stabilized by heating it to a 35 °C setpoint using a Minco CT335 heater controller. The temperature of the SiPM is monitored with a 10K thermistor mounted adjacent to the heater. Temperature of the detector is held to within 0.1 °C of the setpoint using the Minco controller.

3.2 Flow system

The PCAND instrument uses a small, 12 volt diaphragm pump (Parker E134-11-120) to achieve a 1.4 standard liters per minute (SLM) flow rate. Flush time is approximately 3 seconds as evident from Fig. 4. A 3-way valve (ASCO 411L3212HV) is used to switch the flow between sample air and scrubbed air (via an inline charcoal filter). The charcoal filter removes any NO_2 from the flow and gives the I_0 (reference) measurement every 30 seconds for 5 seconds, leaving sample air measurements 50 seconds out of every minute.

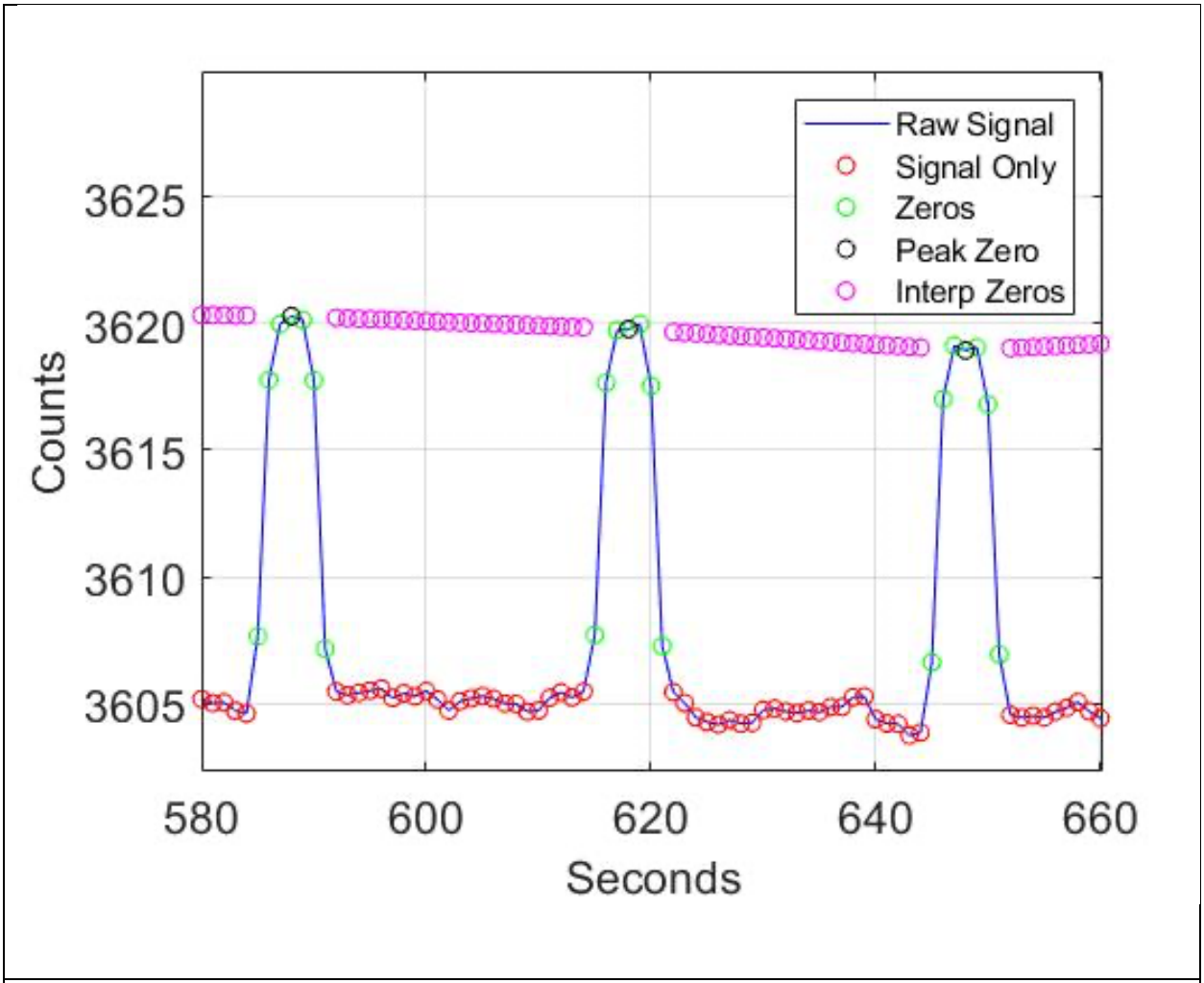

Figure 4. Cadence used to make real-time measurements of I_Z (signal with no absorbers) vs I (signal with absorbers) is 7 seconds for I_Z and 23 seconds for I. We found this was a good cadence allowing 3 seconds to achieve peak I_Z and 3 seconds to return to I. A charcoal filter is switched into the airflow to achieve the I_Z measurement.

We expect a small interference from water vapor. H2O vapor has a cross-section of 3 x 10^{-27} cm^2 /molecule at 405 nm (Lampel *et al.*, 2015; 2017). An atmospheric abundance of H_2O = 1% contributes the same absorption as 50 pptv of NO_2. In addition, we notice stronger attenuation that is not consistent with gas phase absorption like that reported in ozone instruments using UV absorption (Wilson *et al.*, 2006). In principle the presence of water vapor should not affect the measurement if the abundance is constant between the sample and the scrubbed air.

However, the scrubber material (activated charcoal) can add or remove water vapor to the sampled air depending on the prior humidity. Because of this interference, water vapor is removed using two 30 cm lengths of 0.3 cm diameter Nafion Dewline tubing held in an enclosure with Drierite. The dry air sample eliminates any contribution of water vapor in the measurement.

PCAND uses fluorinated ethylene propylene (FEP) lined thermoplastic tubing for all internal plumbing and nylon fittings are used for connections. A 2-micron teflon membrane filter is positioned immediately before the cell inlet to keep small particles from entering the cell and potentially dirtying the mirrors. The loss of NO_2 on the surfaces of the tubing, valve, filter, Nafion, and cell was measured to be less than 0.1 ppb.

3.3 Data acquisition

PCAND uses an Arduino MKR Zero microcontroller for 3-way valve control, LED modulation, and data acquisition. Arduino actuation of the valve is made through a CoolCube R valve controller, which reduces the holding current needed to keep the valve in its open state. LED modulation is produced by the Arduino through the LED controller at a 100 Hz rate. This modulation has a 70% duty cycle used to achieve a digital lock-in to remove any background light from the absorption measurement. We oversample the absorption signal 42k samples / second to increase the native Arduino internal 12-bit measurement to an effective (averaged over a second) ~21-bit measurement. Data is recorded both to an SD card and sent to an RS-232 port. The latter is useful for both instrument testing and for connecting to an external iMet radiosonde where the data is merged for RF data downlink by the radiosonde.

3.4 Data processing

The PCAND absorbance calculation uses equation 1, but accounts for the differential cell pressure between the sample flow and the zero flow, which is restricted by the scrubber. Including the Rayleigh scattering for both zero air and sample air, Eq. 1 is rewritten as equation 4 (Min *et al.* 2016 ; Hannun *et al*., 2020) :

$$\alpha_{NO2} = \left(\frac{I_Z}{I} - 1\right)\left(\alpha_{cav} + \alpha_{Ray,Z}\right) + \Delta\alpha_{Ray} \quad (4)$$

$$\Delta\alpha_{Ray} = \alpha_{Ray,Z} - \alpha_{Ray,\mathrm{S}} \quad (5)$$

$$\alpha_{Ray} = N_{air}\sigma_{Ray} \quad (6)$$

$$\alpha_{NO2} = N_{NO2}\sigma_{NO2} \quad (7)$$

Zero air is NO_2 scrubbed air where I_Z substitutes for I_0 (from equation 1). Rayleigh cavity extinction is broken into 2 parts ($\alpha_{Ray,Z}$ and $\alpha_{Ray,S}$) describing zero air and sample air cavity extinction respectively. In both cases, the Rayleigh scattering cross-section (σ_{Ray}), weighted by the SiPMT response curve (Fig. 3), is used (Bucholtz, 1995). The NO_2 number density (concentration) is found by knowing the absorption cross-section of NO_2 (σ_{NO2}) (Vandalae, 1998).

By varying the pressure of the cell with zero air, we can extrapolate a value for I_0. Substituting I_0 for I_Z in equation 4, we arrive at equation 8. At vacuum (I_0), both $\alpha_{Ray,Z}$ terms go to zero. The α_{NO2} term also goes to zero with no NO_2 in zero air.

$$\alpha_{Ray,S} = \left(\frac{I_0}{I} - 1\right)\alpha_{cav} \quad (8)$$

4 Performance

4.1 Sensitivity and calibration

The PCAND effective pathlength of the optical cavity determines the instruments sensitivity to NO_2. Highly reflective mirrors on either end of the cavity are statically mounted, so no adjustment of their position is required. In practice, the alignment is stable over months of operation. After the initial alignment, calibration is needed to determine the effective pathlength given the mirror positions. Equation 4 can be used with known quantities of NO_2 to determine the effective pathlength (Fig. 5a). Additionally, Rayleigh scattering alone can be used to solve for effective pathlength (Fig. 5b). This requires varying the pressure of zero air (in the absence of NO_2) to generate a data set of absorption attenuation (I) vs number density of zero air. It also requires we solve for equation 8 after it has been reduced from equation 4. To do this, an assumption is

made that $\alpha_{Ray,Z}$ is taken at vacuum, so $\alpha_{Ray,Z}$ goes to zero leaving only $\alpha_{Ray,S}$. Therefore, (I_Z) is calculated at vacuum from the data set. Equation 8 is left to solve for effective pathlength (equation 3). Using known quantities of NO_2 (and equation 4) yields a pathlength of 519 ± 2 m. Using the Rayleigh scattering method and equation 8 yields a pathlength of 524 ± 1 m. The two methods of calibration are within < 1% of each other and both yield pathlengths that agree to within 2σ uncertainty for each fit. Therefore, we choose to use the Rayleigh scattering method in future calibrations (when needed) of PCAND. Note that due to the small Rayleigh cross-section of air at 408 nm, sigma = 1.5 x 10^{-26} cm^{-2} /molecule (Bucholz, 1995) the calibration using air is susceptible to leaks and contamination. Adequate care must be taken to ensure that the system is free of leaks and that the air is pure. In practice, curvature in the Rayleigh calibration curve indicate the presence of a leak or contamination.

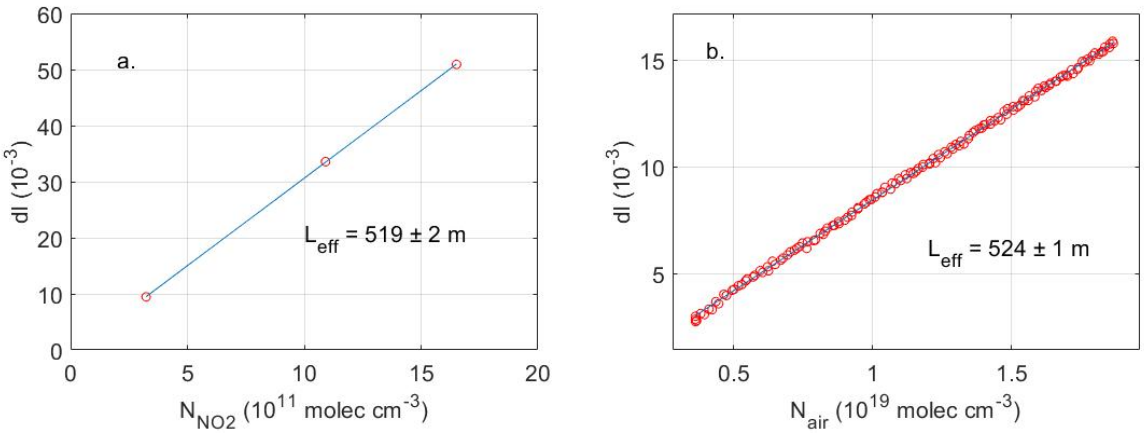

Figure 5. PCAND calibration: a) The effective pathlength (L_{eff}) as determined by attenuation (Attn) due to known additions of NO_2 from a reference tank of NO_2 mixed with zero air. The slope yields the effective pathlength as determined from Equation 1 in the text using the known NO_2 absorption cross section; b) Attenuation due to Rayleigh scatter over a range of cell pressures. The slope of attenuation as a function of number density gives the pathlength using the known Rayleigh scattering cross-section for zero air. The pathlength from each calibration agreed to within 2σ uncertainty for each fit.

225

226 **4.2 Precision and accuracy**

227 The PCAND precision was determined by flowing zero air (under constant pressure of 920 mbar)
228 into the cavity for 2 hours while accumulating 1Hz data. Figure 6 is an Allan deviation plot showing
229 a 1 Hz precision of 94 pptv and a 10 s precision of 30 pptv. The 1 Hz precision translates to 2.3 x
230 10^9 molecules cm^{-3} of NO_2 at 1 atmosphere.

231

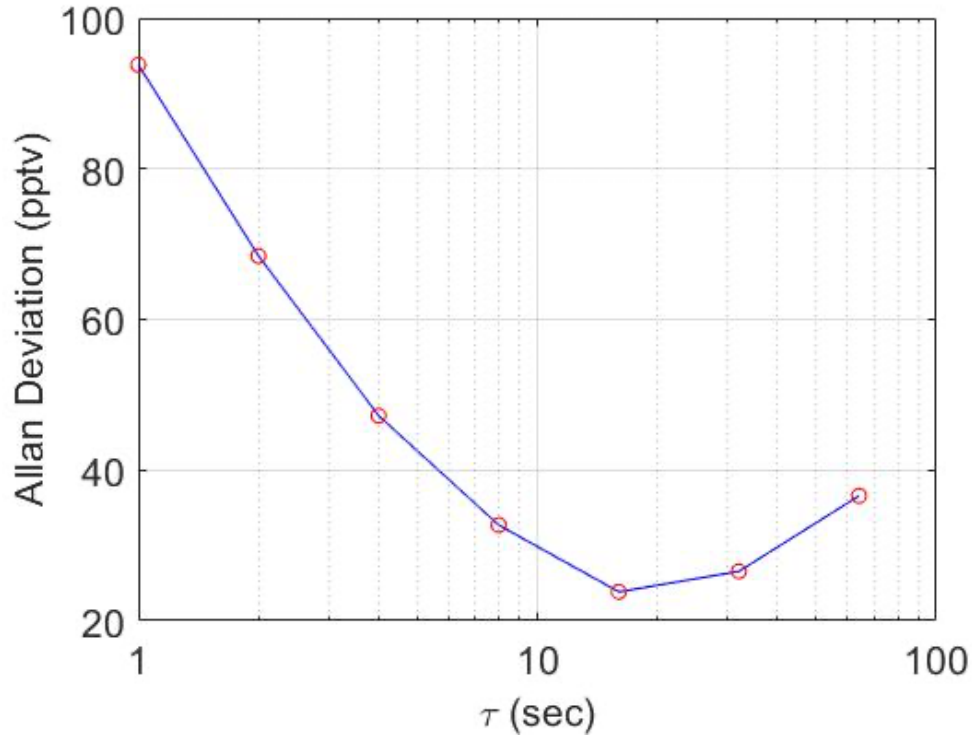

Figure 6. Allan deviation plot for 2 hours of sampling zero air at constant pressure (940 mbar). The Allan deviation is expressed in pptv equivalents of NO_2 as a function of the integration time τ. The curve shows a precision of 94 pptv at 1 second integration time.

232

233 The accuracy of PCAND measurements depends on NO_2 and Rayleigh cross section uncertainties,
234 pressure sensor uncertainty, thermistor uncertainty, and cavity extinction uncertainty. The NO_2
235 absorption cross-section uncertainty is reported to be 3% (Spinei, 2014; Vandalae 1998). A 3%

Rayleigh scattering cross-section uncertainty (Bucholtz, 1995) was used. Taken from data sheets, a conclusion was made that temperature and pressure measurements have uncertainties of 0.5% and 2% respectively. Cavity extinction slope uncertainty was measured at 1%. Together, the total uncertainty (when propagated through equation 4) comes to 6% when applied to the final NO_2 number density.

4.3 Response time

Response time is a direct function of gas flush time in our cell given our small vacuum pump. A flow rate of 1.4 SLM is achieved with the pump resulting in a response time of approximately 3 seconds (Fig. 4). Given a cadence of 5 second zero followed by 25 second sample, one can see (by eye) it takes ~3 seconds for the signal to stabilize with zero air. A larger pump could shorten this response time at the expense of more mass and power needed.

4.4 Photolysis Effects

The photolysis quantum yield is 0.22 at 408 nm (*Troe, 2000)*, so we expect some fraction of the NO_2 in the cell to photolyze, $NO_2 + hv \rightarrow NO + O$. In static cells the photolysis of NO_2 has been shown to be a concern (Platt *et al., 2019*) In the case of our detection, it is unlikely that a significant fraction of NO_2 will be photolyzed because the sample flows through the cell quickly with a flush time of approximately 1 s and the number of photons available for photolysis is small.

We can estimate the number of photons in the cell from the detector signal. The SiPM has a radiant sensitivity of 4×10^5 A/W and a photon detection efficiency of 50%. Based on our detection signal of 2×10^{-5} A, we estimate the optical power is roughly 10^{-10} W and calculate a photon flux of 2×10^9 photons/s. A typical absorbance with 1 ppb NO_2 in the cell is 10^{-3}, thus we expect that roughly 2×10^6 photons/s are absorbed by the 1 ppb NO_2 in the cell. At 900 hPa the number density of 1 ppb NO_2 is roughly 2.2×10^{10} molecules/cm^3. The absorption of 2×10^6 photons would result in the photolysis of 4.4×10^5 NO_2 molecules, or 2×10^{-5} of the available NO_2 molecules. While this number is quite low for our conditions, it is worth noting that with slower flows and higher photon fluxes the photolysis could be significant and secondary chemistry could be a concern.

5 Field demonstration

PCAND was launched on 3 low altitude (~7 km) balloon flights for demonstration purposes during the summer of 2022. PCAND was physically linked (via RS232 cable) to a commercial weather sonde for real-time data downlink (via the weather sonde). Results from the flight (Fig. 7) launched on 18 August 2022 show a vertical profile of NO_2 indicative of that time of year with high concentrations of NO_2 near the ground. This flight occurred at 8 am local time when the boundary layer was still close to the ground. The temperature deviation in the instrument box during flight to 7km was less than 1 °C.

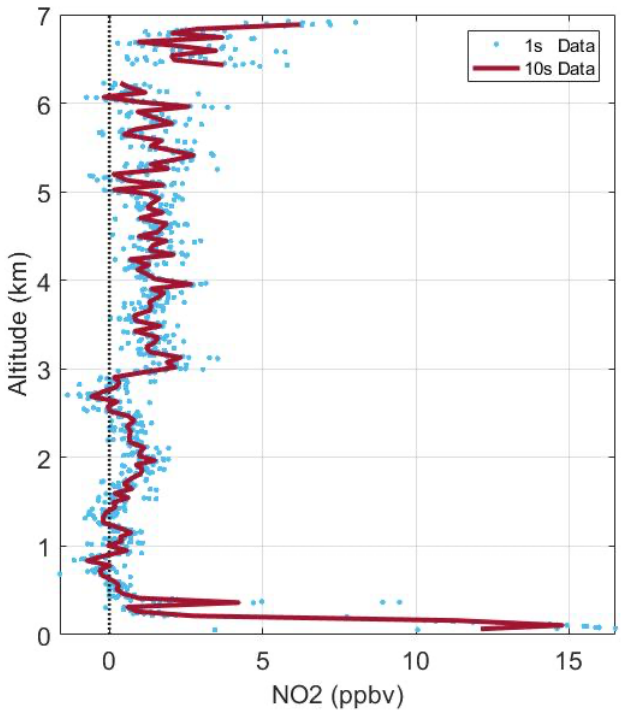

Figure 7. PCAND flight data from 18 August 2022 balloon launch. Programmed cut-down of balloon at 7 km to achieve payload recovery. Significant concentrations of NO_2 appear near the surface and again at cut-down (~7 km) altitude.

5.1 Validation with CANOE

PCAND was validated with another NO_2 instrument called CANOE (Compact Airborne Nitrogen diOxide Experiment). CANOE was based on the design of a similar instrument called CAFE (St. Clair *et al.*, 2019) (Compact Airborne Formaldehyde Experiment). The only difference between CANOE and CAFE are the laser wavelengths (532 nm for CAFE vs 355 nm for CANOE) and PMT detectors used. CANOE is an LIF instrument which has been deployed on several airborne campaigns including Dynamics and Chemistry of the Summer Stratosphere (DCOTSS) and Fire Influence on Regional to Global Environments and Air Quality (FIREX-AQ). CANOE has been calibrated to known cylinders of NO_2 concentration. Fig. 8 shows a ~4-hour data set where PCAND and CANOE shared the same inlet port sampling the air during a morning in the DC greater metropolitan area. Clearly, a rush hour peak of NO_2 is seen trailing off by noon. Fig. 8b shows good agreement between the measurements with a slope of 0.94 $\pm$ 0.004 and an intercept of 0.09 $\pm$ 0.012 ppbv NO_2 (r^2 = 0.96).

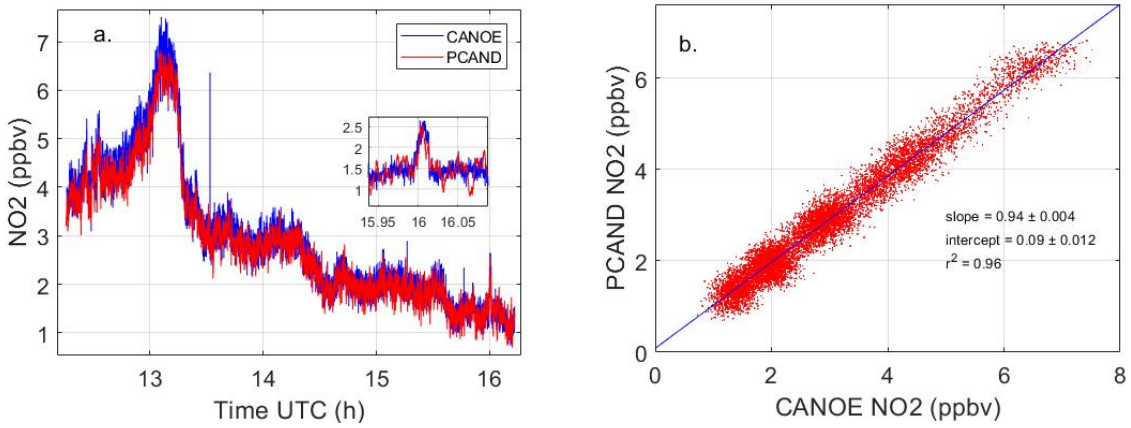

Figure 8. PCAND and CANOE measurements during rush hour at GSFC on 14 July 2023. a) Comparison over ~4 hours which clearly shows rush hour peak around ~13 UTC. b) Scatter

plot of the same data showing high correlation between instrument measurements. A linear fit to the data gives a slope of 0.94 $\pm$ 0.004 and an intercept of 0.09 $\pm$ 0.012 ppbv with an r^2 = 0.96.

6 Summary and conclusions

PCAND provides very high sensitivity to NO_2 for such a small package using broadband cavity-enhanced UV absorption at 408 nm. PCAND has a precision of ~94 pptv s^{-1} with an accuracy of 6.0%. Although PCAND was designed for portable, battery powered operation (as needed for a balloon flight), it could easily be used in either ground or lab-based measurements. It was successfully tested on 3 balloon flights. A comparison with another (calibrated) NO_2 instrument (CANOE) showed strong agreement over a ~4-hour period.

Author contributions. SAB performed the investigation, controller software, electronics design, testing, and wrote the paper. RAH wrote the signal processing code and determined the best wavelength to use for NO_2 absorption. AKS did all the mechanical design including optical plate, fixtures, and cell. TFH determined the correct mirrors to use, consulted with AKS on the optical layout, and made the science case for receiving funding for this work.

Competing interest. At least one of the (co-)authors is a member of the editorial board of Atmospheric Measurement Techniques.

Acknowledgements. The balloon flights were made at the Howard University Beltsville Campus with the help of Adrian Flores. We would additionally like to thank Ryan Stauffer for his expertise in balloon flight needed to launch and recover our instrument.

Financial support. This research has been supported by the NASA Internal Research and Development (IRAD) program at Goddard Space Flight Center (GSFC).

References

Ball, S. M., Langridge, J. M., and Jones, R. L.: Broadband cavity enhanced absorption spectroscopy using light emitting diodes, Chem. Phys. Lett., 398, 68–74, https://doi.org/10.1016/j.cplett.2004.08.144, 2004.

Bucholtz, A.: Rayleigh-scattering calculations for the terrestrial atmosphere, Appl. Optics, 34, 2765–2773, https://doi.org/10.1364/AO.34.002765, 1995.

Cersosimo, A., Serio, C., and Masiello, G.: TROPOMI NO2 Tropospheric Column Data: Regridding to 1 km Grid-Resolution and Assessment of their Consistency with In Situ Surface Observations, Remote Sens., 12, 2212, https://doi.org/10.3390/rs12142212, 2020.

Cooper, M. J., Martin, R. V., Henze, D. K., and Jones, D. B. A.: Effects of a priori profile shape assumptions on comparisons between satellite NO2 columns and model simulations, Atmos. Chem. Phys., 20, 7231–7241, https://doi.org/10.5194/acp-20-7231-2020, 2020a.

Cooper, M. J., Martin, R. V., McLinden, C. A., and Brook, J. R.: Inferring ground-level nitrogen dioxide concentrations at fine spatial resolution applied to the TROPOMI satellite instrument, Environ. Res. Lett., 15, 104013, https://doi.org/10.1088/1748-9326/aba3a5, 2020b.

Dang, R., Jacob, D. J., Shah, V., Eastham, S. D., Fritz, T. M., Mickley, L. J., Liu, T., Wang, Y., and Wang, J.: Background nitrogen dioxide (NO2) over the United States and its implications for satellite observations and trends: effects of nitrate photolysis, aircraft, and open fires, Atmos. Chem. Phys., 23, 6271–6284, https://doi.org/10.5194/acp-23-6271-2023, 2023.

Duncan, B. N., Lamsal, L. N., Thompson, A. M., Yoshida, Y., Lu, Z., Streets, D. G., Hurwitz, M. M., and Pickering, K. E.: A space-based, high-resolution view of notable changes in urban NOx pollution around the world (2005–2014), J. Geophys. Res.-Atmos., 121, 976–996, https://doi.org/10.1002/2015JD024121, 2016.

Fiedler, S. E., Hese, A., and Ruth, A. A.: Incoherent broad-band cavity-enhanced absorption spectroscopy, Chem. Phys. Lett., 371, 284–294, https://doi.org/10.1016/S0009-2614(03)00263-X, 2003.

Hannun, R. A., Swanson, A. K., Bailey, S. A., Hanisco, T. F., Bui, T. P., Bourgeois, I., Peischl, J., and Ryerson, T. B.: A cavity-enhanced ultraviolet absorption instrument for high-precision, fast-time-response ozone measurements, Atmos. Meas. Tech., 13, 6877–6887, https://doi.org/10.5194/amt-13-6877-2020, 2020.

Lampel, J., Pöhler, D., Tschritter, J., Frieß, U., and Platt, U.: On the relative absorption strengths of water vapour in the blue wavelength range, Atmos. Meas. Tech., 8, 4329–4346, https://doi.org/10.5194/amt-8-4329-2015, 2015.

Lampel, J., Pöhler, D., Polyansky, O. L., Kyuberis, A. A., Zobov, N. F., Tennyson, J., Lodi, L., Frieß, U., Wang, Y., Beirle, S., Platt, U., and Wagner, T.: Detection of water vapour absorption around 363 nm in measured atmospheric absorption spectra and its effect on DOAS evaluations, Atmos. Chem. Phys., 17, 1271–1295, https://doi.org/10.5194/acp-17-1271-2017, 2017.

Martin, R. V., Jacob, D. J., Chance, K., Kurosu, T. P., Palmer, P. I., and Evans, M. J.: Global inventory of nitrogen oxide emissions constrained by space-based observations of NO2 columns, J. Geophys. Res.-Atmos., 108, https://doi.org/10.1029/2003JD003453, 2003.

Min, K.-E., Washenfelder, R. A., Dubé, W. P., Langford, A. O., Edwards, P. M., Zarzana, K. J., Stutz, J., Lu, K., Rohrer, F., Zhang, Y., and Brown, S. S.: A broadband cavity enhanced absorption spectrometer for aircraft measurements of glyoxal, methylglyoxal, nitrous acid, nitrogen dioxide, and water vapor, Atmos. Meas. Tech., 9, 423–440, https://doi.org/10.5194/amt-9-423-2016, 2016.

Miyazaki, K., Eskes, H., Sudo, K., Boersma, K. F., Bowman, K., and Kanaya, Y.: Decadal changes in global surface NOx emissions from multi-constituent satellite data assimilation, Atmos. Chem. Phys., 17, 807–837, https://doi.org/10.5194/acp-17-807-2017, 2017.

Platt, U. and Kuhn, J.: Caution with spectroscopic NO2 reference cells (cuvettes), Atmos. Meas. Tech., 12, 6259–6272, https://doi.org/10.5194/amt-12-6259-2019, 2019.

Ryerson, T. B., Williams, E. J., and Fehsenfeld, F. C.: An efficient photolysis system for fast-response NO2 measurements, J. Geophys. Res.-Atmos., 105, 26447–26461, https://doi.org/10.1029/2000JD900389, 2000.

Sluis, W. W., Allaart, M. a. F., Piters, A. J. M., and Gast, L. F. L.: The development of a nitrogen dioxide sonde, Atmos. Meas. Tech., 3, 1753–1762, https://doi.org/10.5194/amt-3-1753-2010, 2010.

Spinei, E., Cede, A., Swartz, W. H., Herman, J., and Mount, G. H.: The use of NO2 absorption cross section temperature sensitivity to derive NO2 profile temperature and stratospheric–tropospheric column partitioning from visible direct-sun DOAS measurements, Atmos. Meas. Tech., 7, 4299–4316, https://doi.org/10.5194/amt-7-4299-2014, 2014.

St. Clair, J. M., Swanson, A. K., Bailey, S. A., and Hanisco, T. F.: CAFE: a new, improved nonresonant laser-induced fluorescence instrument for airborne in situ measurement of formaldehyde, Atmos. Meas. Tech., 12, 4581–4590, https://doi.org/10.5194/amt-12-4581-2019, 2019.

Thornton, J. A., Wooldridge, P. J., and Cohen, R. C.: Atmospheric NO2: In Situ Laser-Induced Fluorescence Detection at Parts per Trillion Mixing Ratios, Anal. Chem., 72, 528–539, https://doi.org/10.1021/ac9908905, 2000.

Troe, J.: Are Primary Quantum Yields of NO2 Photolysis at λ ≤ 398 nm Smaller than Unity?, Z. Phys. Chem., 214, 573–581, https://doi.org/10.1524/zpch.2000.214.5.573, 2000.

Vandaele, A. C., Hermans, C., Simon, P. C., Carleer, M., Colin, R., Fally, S., Mérienne, M. F., Jenouvrier, A., and Coquart, B.: Measurements of the NO2 absorption cross-section from 42 000 cm−1 to 10 000 cm−1 (238–1000 nm) at 220 K and 294 K, J. Quant. Spectrosc. Ra., 59, 171–184, https://doi.org/10.1016/S0022-4073(97)00168-4, 1998.

Washenfelder, R. A., Langford, A. O., Fuchs, H., and Brown, S. S.: Measurement of glyoxal using an incoherent broadband cavity enhanced absorption spectrometer, Atmos. Chem. Phys., 8, 7779–7793, https://doi.org/10.5194/acp-8-7779-2008, 2008.

Wilson, K. L. and Birks, J. W.: Mechanism and Elimination of a Water Vapor Interference in the Measurement of Ozone by UV Absorbance, Environ. Sci. Technol., 40, 6361–6367, https://doi.org/10.1021/es052590c, 2006.

Womack, C. C., Brown, S. S., Ciciora, S. J., Gao, R.-S., McLaughlin, R. J., Robinson, M. A., Rudich, Y., and Washenfelder, R. A.: A lightweight broadband cavity-enhanced spectrometer for NO2 measurement on uncrewed aerial vehicles, Atmos. Meas. Tech., 15, 6643–6652, https://doi.org/10.5194/amt-15-6643-2022, 2022.